Nanoscale

RSC Publishing

PAPER

View Article Online
View Journal | View Issue

Cite this: *Nanoscale*, 2013, **5**, 2394

Facile synthesis of Cu and Cu@Cu–Ni nanocubes and nanowires in hydrophobic solution in the presence of nickel and chloride ions†

Huizhang Guo, Yuanzhi Chen,* Hemei Ping, Jiarui Jin and Dong-Liang Peng*

Received 12th October 2012
Accepted 3rd January 2013

DOI: 10.1039/c3nr33142c

www.rsc.org/nanoscale

A highly shape selective synthesis of Cu and Cu@Cu–Ni nanocubes and nanowires has been developed by modulating the coordination chemistry of transition metal ions with a trioctylphosphine (TOP)–Cl^- ligand pair in oleylamine under mild organic solvent conditions. The as-prepared nanocubes have a face-centered cubic (fcc) phase and are covered by six {100} facets, whereas the as-prepared nanowires have a multi-twinned structure and grow along the [110] direction. Both the Ni^{2+} and Cl^- ions, along with TOP, play vital roles in determining the final morphology of the as-prepared nanocrystals (NCs). TOP can be used to selectively generate single-crystal seeds at the initial stage, which then grow into nanocubes in the presence of Cl^- ions, while the absence of TOP leads to the formation of multi-twined crystal seeds that finally develop into nanowires. Moreover, Ni can be incorporated to form a Cu–Ni alloy shell over a Cu core at higher temperatures in a one-pot process, which makes diamagnetic Cu NCs magnetically responsive and has a significant influence on their optical properties.

Introduction

The shape- and morphology-controlled synthesis of transition metal nanocrystals (NCs) by a facile and reliable synthetic procedure has received intensive attention in recent years. In the past decade, important progress has been made in understanding of the formation mechanism and the controllable synthesis of metal NCs in colloidal solutions, especially noble metal NCs with an anisotropic morphology.[1–3] However, compared to a larger number of reports on the shape-controlled synthesis of noble metal NCs, such as Ag,[4,5] Au,[6] Pt[7] and Pd,[8] only a few have described the successful preparation of transition metal NCs with specific shapes.[9–11] This lack of success is partially attributed to the shape control of NCs being a kinetically controlled process instead of a thermodynamically controlled one.[12] Because of their low electrode potential, strong reducing agents are required to reduce transition metal ions into zero-valence monomers which are the basic building units in the following nucleation and growth steps. Nevertheless, the reduction kinetics might become incontrollable because of the use of strong reducing agents. Therefore, etchants[13–15] [*e.g.* Fe(III) species] and capping agents[9,16] (*e.g.* hydrogen) should be introduced into the synthesis to achieve anisotropic NCs with specific facets and morphologies. Recently, the impact of halide ions on the final morphology of metal NCs has been noticed. Xia *et al.* reported that bromide ions led to the selective initiation of the galvanic replacement of Pd NCs and promoted the formation of anisotropic Pd–Pt bimetallic NCs.[17] Sun and Peng synthesized Ag nanocubes in a hydrophobic solvent in the presence of Cl^- ions.[18] The research of Shevchenko *et al.* also indicated that Co^{2+} ions adsorbed on the surface of $CoPt_3$ seeds could promote the formation of $CoPt_3$–Au dumbbells while Cl^- ions could inhibit the growth of Au domains in the formation of $CoPt_3$–Au dumbbells.[19]

Cu, which is much cheaper than Au, Ag, Pt and Pd, is one of the most important industrial metals. Cu nanowires have a great potential to be exploited in electronics to produce transparent and flexible conducting films to replace ITO for flexible displays because of their acceptable electric conductivity and transmittance.[20,21] Cu NCs have also been used as catalysts in methanol synthesis[22] and hydrogen production by water-gas-shift.[23] However, reports on the reliable and facile method for the preparation of Cu NCs with specific shapes are not common. Some studies have reported the synthesis of Cu-containing NCs, such as Cu–Ni alloy NCs,[24] monodisperse intermetallic Cu–Au NCs,[25] Au–Cu alloy monodisperse nanocubes,[12] Cu–Ni core–shell nanoparticles,[26] Cu–Ni core–shell nanowires[27] and Au@Cu core–shell NCs.[28] More recently, Xia's group reported an aqueous method for the shape-controlled synthesis of Cu nanocubes and nanowires.[29]

Herein, we disclose an alternative nonaqueous method, not only for the highly shape selective synthesis of Cu nanocubes and nanowires, but also for the formation of bimetallic

Department of Materials Science and Engineering, College of Materials, Xiamen University, Xiamen, 361005, P. R. China. E-mail: yuanzhi@xmu.edu.cn; dlpeng@xmu.edu.cn; Fax: +86 592 2183515; Tel: +86-592-2188025

† Electronic supplementary information (ESI) available: Related synthetic details, SEM images, TEM images, EDS spectra, size-distribution histogram, color photos at different reaction stages, UV-Vis spectra, Auger spectra and magnetic measurement results. See DOI: 10.1039/c3nr33142c

core–shell structured (Cu@Cu–Ni) magnetic nanocubes and nanowires. The formation mechanism on the growth of nanocubes and nanowires has also been explored in this report, which may offer useful references for the shape-controlled synthesis of transition metal NCs and bimetallic core–shell nanostructures. Moreover, the impact of the growth of the magnetic shell over Cu core on the optical and magnetic properties of the as-prepared NCs has also been investigated. The combination of magnetic metal components with Cu NCs brings multi-functionalities for the NCs, which broadens their practical applications.

Experimental section

1 Synthesis

Chemicals. Nickel(II) acetylacetone [$Ni(acac)_2$, 95%, Strem Chemicals Inc.], copper(II) chloride dihydrate ($CuCl_2 \cdot H_2O$, AR, SCRC), oleylamine (80–90%, Acros Organics), trioctylphosphine (TOP, 97%, Strem Chemicals Inc.), copper(II) nitrate trihydrate [$Cu(NO_3) \cdot H_2O$, AR, Xilong Chemical Co., Ltd.], hexane (AR, SCRC), toluene (AR, SCRC), and trichloromethane ($CHCl_3$, AR, SCRC) were all used as received without any further purification.

Synthesis of Cu nanocubes. In a typical synthesis, 0.4 mmol of $Ni(acac)_2$ and 0.8 mmol of $CuCl_2 \cdot H_2O$ were dissolved in 7 ml of oleylamine in a three-necked flask and kept under a flow of high-purity argon gas at 80 °C for 20 min with strong magnetic stirring before 1 mmol of TOP was injected. After stirring for 5 min, the resulting solution was then heated to 180 °C rapidly and kept at this temperature for 4 h. After cooling to room temperature naturally, excess hexane was added to the black solution to give a black precipitate which was isolated *via* centrifugation (4000 rpm for 5 min). The precipitate was then washed with a mixture of hexane and trichloromethane, and dried in a vacuum drying oven for 1 h to obtain a dry powder.

Synthesis of Cu nanowires. In a typical synthesis of Cu nanowires with a diameter of 16 nm, 0.4 mmol of $Ni(acac)_2$ and 0.8 mmol of $CuCl_2 \cdot H_2O$ were dissolved in 10 ml of oleylamine in a three-necked flask and kept under a flow of high-purity argon gas at 80 °C for 20 min with strong magnetic stirring. After that, the resulting solution was then heated to 170 °C rapidly and kept at this temperature for 4 h. The subsequent cleaning procedures were the same as those for the Cu nanocubes, except for the centrifugation rate, which was 10 000 rpm for 10 min. For the synthesis of Cu nanowires with a diameter of 22 nm, we decreased the amount of oleylamine to 7 ml while we increased the reaction temperature to 180 °C.

Synthesis of Cu@Cu–Ni nanocubes. Cu@Cu–Ni nanocubes were prepared by modifying the procedure of synthesis of Cu nanocubes. After aging the mixed solution at 180 °C for 4 h, the reaction temperature was increased to 210 °C slowly (5 °C per min) and aging at this temperature for 1 h. After cooling down to room temperature naturally, similar cleaning steps as those for Cu nanocubes were applied.

Synthesis of Cu@Cu–Ni nanowires. Cu@Cu–Ni nanowires were prepared by modifying the procedure used for the synthesis of the Cu nanowires. After aging the mixed solution at 170 °C for 4 h, the reaction temperature was increased to 210 °C slowly (5 °C per min) and aged at this temperature for 1 h. After cooling to room temperature naturally, similar cleaning steps as those used for the Cu nanowires were applied.

2 Characterization

Transmission electron microscopy (TEM). A portion of the as-prepared powders was dispersed in toluene *via* ultrasound concussion for 15 min. The TEM samples were prepared by dropping the particle suspensions in toluene onto a gold grid coated with carbon film before drying at room temperature under ambient conditions. TEM images, energy dispersive X-ray spectroscopy (EDS) data and selective area electron diffraction (SAED) data were collected on a JEM-2100 transmission electron microscope operating at 200 kV. EDS line-scan analysis and mapping were performed on a TECNAI F-30 transmission electron microscope equipped with a scanning TEM (STEM) unit and a high-angle annular dark-field (HAADF) detector operated at 300 kV.

Scanning electron microscopy (SEM). The samples for SEM observation were prepared by dropping the powder suspensions in toluene onto a silicon wafer before drying at room temperature under ambient conditions. The SEM images were collected on a Hitachi S-4800 scanning electron microscope operated at 20 kV.

X-ray diffraction (XRD). The samples for XRD analyses were prepared by dropping the powder suspensions in toluene onto a glass wafer before drying at room temperature under ambient conditions. XRD measurements were taken on a Panalytical X'pert PRO diffractometer using Cu Kα radiation, operating at 40 kV and 30 mA.

Auger electron spectroscopy (AES). AES experiments were carried out using a PHI-610 scanning Auger microprobe. A coaxial electron gun with a single pass and 0.3% of the energy resolution selection of cylindrical mirror analyzer (CMA) were employed. The primary electron beam energy of 3 keV and the emission current of 0.1 mA were selected.

Fourier transform infrared (FT-IR) spectroscopy. FTIR spectra were recorded using a Nicolet IS10 FT-IR spectrometer.

Optical spectra data. Visible-Near Infrared (NIR) extinction spectra were obtained at room temperature with a Shimadzu UV-2550 ultraviolet-visible spectrophotometer.

Magnetic measurements. Approximately 10 mg of powder sample was weighed into a gelatin capsule. Magnetic measurements were carried out with a superconducting quantum interference device magnetometer (SQUID, MPMS-5) in the temperature range of 5–300 K. During the ZFC-FC experiments the measuring field and cooling field are 100 Oe.

Results and discussions

Synthesis and characterization of Cu nanocubes

Cu nanocubes were synthesized by a one-pot reaction using copper(II) chloride dihydrate ($CuCl_2 \cdot 2H_2O$) and nickel(II) acetylacetone [$Ni(acac)_2$] as metal precursors in the presence of oleylamine and trioctylphosphine (TOP) at 180 °C (see

Experimental section for synthetic details). The representative SEM and TEM images of the Cu nanocubes are shown in Fig. 1a and b which demonstrate that the products are all cubes with an edge length of 60 ± 8 nm (see Fig. S1 in ESI†), and no other morphology can be observed, indicating a relatively good uniformity. The SAED pattern (Fig. 1c) acquired from an individual Cu nanocube (Fig. 1c inset) exhibits diffraction spots corresponding to face-centered cubic (fcc)-structured Cu viewed down the [100] zone axis. A similar SAED pattern can be revealed for every examined Cu nanocube without exception, indicating that the as-prepared Cu nanocubes are single crystals covered by six {100} facets. The EDS data (Fig. 1d) recorded from these nanocubes undoubtedly shows the presence of only Cu without any Ni or O (in the limit range of EDS analysis). Fig. 1e shows the XRD pattern of the as-prepared Cu nanocubes. Different from bulk Cu (JCPDS #03-1018), whose strongest XRD diffraction peak is the (111) peak followed by the (200), (220) and (311) peaks, the as-synthesized Cu nanocubes only give the (200) diffraction peak. This is because of their preferential orientation with {100} planes parallel to the substrate.

Synthesis and characterization of Cu nanowires

TOP was found to play an important role in selecting the final morphology of the Cu NCs. When TOP was removed from the reaction, the generated products were dominated by Cu nanowires rather than nanocubes. Fig. 2a and b show the SEM and TEM images of the as-prepared Cu nanowires (see Experimental section for synthetic details). It demonstrates that the products contain about 95% nanowires with a uniform diameter of 15.2 ± 1.8 nm (see Fig. S2,† for detailed size distribution) and entire lengths up to 10 μm (see low-magnification SEM image in Fig. S3†), along with about 5% nanocubes. Different from the Cu nanowires growing from large seeds,[21] which might decrease the transmittance of Cu nanowire films, the as-prepared Cu nanowires do not have large particles attached to the ends. In addition, these nanowires were found to be highly flexible and could be easily bent without being broken, which can be attributed to the presence of a multi-twinned boundary in the nanowire.[30] This indicates that the as-prepared Cu nanowires have a great potential to be used in flexible conducting films. If the reaction temperature was increased to 180 °C and the amount of oleylamine was reduced to 7 ml, the diameter of the as-prepared Cu nanowires would increase to 22 ± 3 nm (see Fig. 1c for TEM image and Fig. S4 in ESI† for size distribution). A ligand exchange process of oleylamine with TOP was applied by adding 1 mmol of TOP into the reaction solution after cooling to room temperature, followed by ultrasound concussion. Once the Cu nanowires were coated with TOP, they were likely to

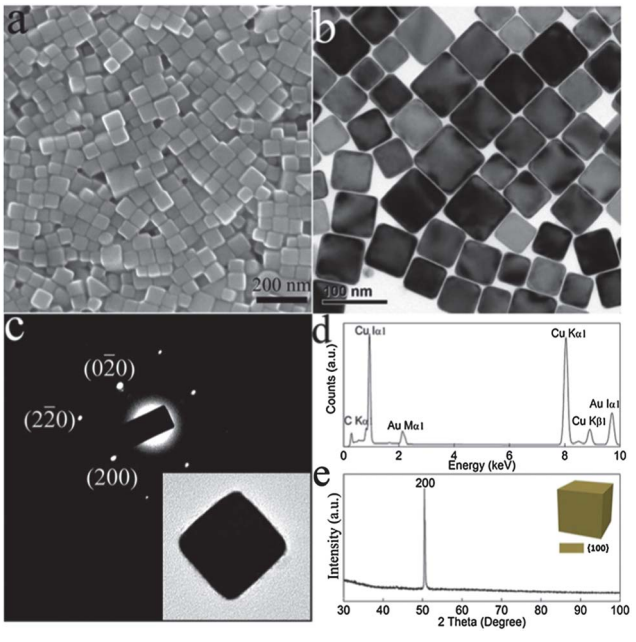

Fig. 1 (a) and (b) are the SEM and TEM images of the as-synthesized Cu nanocubes. (c) SAED pattern of a single Cu nanocube (inset) in the [001] zone axis. (d) and (e) are the EDS spectrum and XRD pattern of the as-synthesized Cu nanocubes, respectively. The inset in (e) is a schematic drawing of a nanocube with exposed facets.

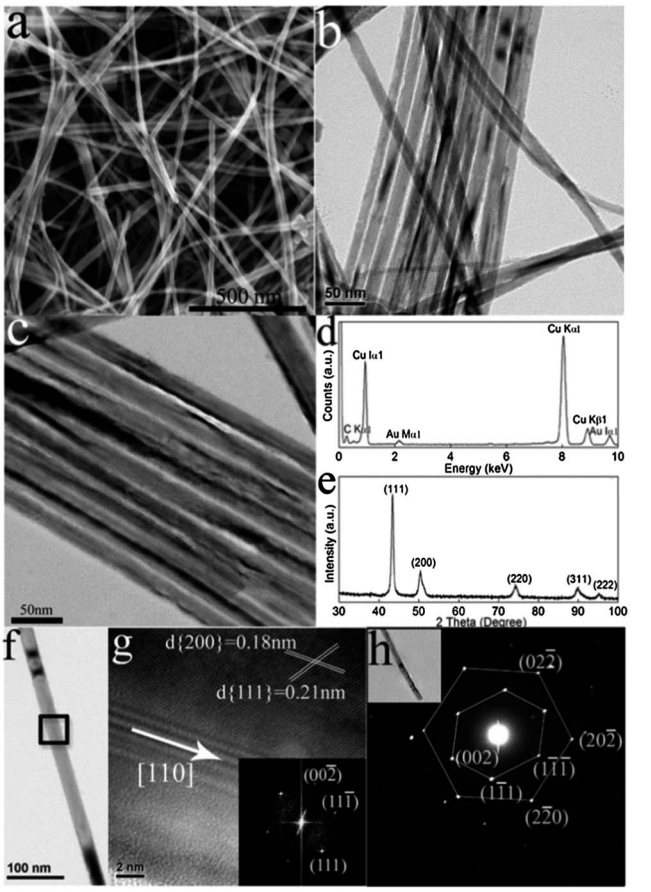

Fig. 2 (a) and (b) are the SEM and TEM images of the as-synthesized Cu nanowires with an average diameter of 15.2 nm. (c) is the TEM image of the Cu nanowires with a diameter of 22 nm. (d) and (e) are the EDS spectrum and XRD pattern of the Cu nanowires with an average diameter of 15.2 nm, respectively. (f) TEM image of an individual Cu nanowire. (g) HRTEM image and corresponding FFT pattern (inset) taken from the marked area in (f). (h) SAED pattern of an individual nanowire (inset). The inner and outer sketched diffraction patterns correspond to the [110] and [111] zone axes, respectively.

self-assemble into straight bundles on the TEM grid (Fig. 2b and c). More importantly, TOP can provide effective surface protection to the Cu nanocubes. Similar to the as-prepared Cu nanocubes, there is neither a characteristic band belonging to Ni nor O in the EDS spectra recorded from these nanowires (Fig. 2d). The XRD pattern acquired from the TOP-coated products, which have been kept in air for a month, is shown in Fig. 2e. It demonstrates five diffraction peaks at $2\theta = 43.4$, 50.4, 74.3, 89.9 and 95.2° which are indexed to the (111), (200), (220), (311) and (222) crystalline planes of fcc Cu (JCPDS #03-1018), respectively. No signals from impurities, such as Cu_2O or Ni were observed, indicating a fairly pure chemical phase. On the contrary, for the Cu nanowires without a coating of dense TOPs after keeping in air for one month,[31] a XRD peak (Fig. S5†) located at 36.8°, which is indexed as (111) crystalline plane of Cu_2O (JCPDS #5-667), occurs that indicates surface oxidization. Fig. 2f and g show the TEM image and high-resolution TEM (HRTEM) image along with the corresponding fast Fourier transfer (FFT) pattern of a single nanowire, respectively. The observed lattice fringes with a spacing of 0.21 and 0.18 nm correspond to the {111} and {200} planes of fcc Cu, respectively. A growth direction of [110] is identified and twinned boundaries can also be clearly observed throughout the HRTEM image. SAED patterns were recorded on individual nanowires to identify the twinned structure within the nanowires. As demonstrated in Fig. 2h, the blended diffraction spots can be viewed as the superposition of the diffraction spots in [110] and [111] zone axes of the fcc structure, indicating a twined structure which was also observed in other metal nanowires.[32,33] Together with HRTEM observation, the diffraction patterns suggests that the as-prepared Cu nanowires are likely to have a five-fold twinned pentagonal structure bounded by five {100} side facets and ten {111} facets at two ends. Such a feature is consistent with the results previously reported for some noble metals such as Pd.[2]

Discussion on the formation mechanism of Cu NCs

Generally, the formation of NCs can be divided into a nucleation step and the following growth of the crystal from the nuclei. However, before the nucleation step, there is the reduction step of the salt precursors into zero-valent monomers, which are the basic building blocks of the NCs and should not be ignored. It should be emphasized that no products would be obtained even at a temperature of 300 °C, if $CuCl_2 \cdot 2H_2O$ was used as a single Cu salt precursor without any $Ni(acac)_2$ in the reaction solution. We attribute it to the formation of stable complexes between Cu^{2+} and halide anions [*e.g.*, $CuCl_4^{2-}$ and $Cu(oleylamine)_2Cl_2$], which prevents Cu^{2+} from being reduced by oleylamine. On the other hand, according to our former study, Ni nanoparticles could not be formed at a temperature below 175 °C in oleylamine.[34] However, when a small amount of $Ni(acac)_2$ was added and the reaction maintained at a relatively low temperature (such as 170 °C) Cu nanocubes with high purity could be obtained. During this reaction process, the mixed solution changed from deep blue, at 80 °C, to light yellow, at 160 °C (Fig. S6†), indicating that stable complexes containing Cu^{2+} were formed. At this temperature, a small amount of Ni^{2+} had been reduced into a Ni^0 species. However, crystal nuclei could not form from these Ni^0 atoms because of the low reaction temperature. The mixed solution turned into a red-brown color when kept at 180 °C for 1 h, implying the formation of a Cu^0 species due to the reduction of Cu^{2+} during the galvanic replacement between Cu^{2+} and the highly active Ni^0 species. An experiment was designed to confirm the galvanic replacement between Ni(0) and Cu^{2+}. Firstly, Ni nanoparticles with a diameter of about 13 nm (see Fig. S7a†) were synthesized. Then they were used as seeds to induce the formation of Cu NCs through the galvanic replacement between Ni and Cu^{2+} (see the ESI† for experimental details). As shown in Fig. S7b–S7d,† the Ni element was almost consumed, owing to the oxidation by Cu^{2+}, as a result Cu–Ni alloyed NPs with much less Ni and an uncontrolled morphology were generated. Based on the above experimental observation, a plausible formation mechanism of the Cu nanocubes and nanowires in the presence of Cl^- anions and Ni^{2+} ions is proposed. We hypothesized that Ni^{2+} ions were reduced into zero-valent monomers by oleylamine at a relatively low temperature which was not thermodynamically satisfactory for the formation of Ni nuclei. Therefore, these Ni^0 atoms with high chemical activity would rapidly reduce Cu^{2+} into Cu^0 with the synergistic effect of oleylamine during a galvanic replacement reaction which was mentioned in former reports.[17,19,35–38] Meanwhile, Ni^0 atoms were oxidized back to Ni^{2+} during this galvanic replacement. As the reiteration of the reduction and galvanic replacement proceeded, the concentration of Cu^0 would increase. Then, as shown in Scheme 1, the Cu nuclei would be formed from these Cu^0 monomers through the nucleation step once the concentration of Cu^0 surpassed the critical nucleation concentration. The combination of reducing Ni^{2+} into Ni^0 and the galvanic replacement between Ni^0 and Cu^{2+} could reduce the formation rate of the Cu^0 atoms so as to keep the nuclei growth under kinetic control. The final morphology (cube or wire) of these Cu NCs depends on the types of crystal seeds used and the selective chemical adsorption of the Cl^- ions.

Effect of TOP on the selective generation of crystal seeds

In order to elucidate the role of TOP in the formation process of Cu NCs, products obtained at different reaction stages were collected for TEM characterization. As shown in Fig. 3a, multi-twined crystal seeds were generated when the reaction was halted immediately once the reaction temperature reached

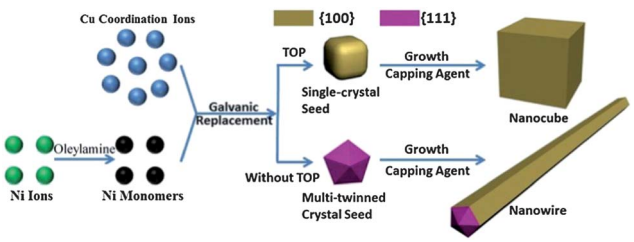

Scheme 1 Schematic illustration for the shape-selective formation of Cu nanocubes and five-fold twinned pentagonal nanowires.

180 °C in the typical synthesis of Cu nanowires. The twined boundary can be clearly observed from the inset of Fig. 3a. Then, these multi-twined crystal seeds would grow into nanowires or nanorods with an average diameter of 13 nm (Fig. 3b). On the other hand, in the presence of TOP, which could coordinate with Ni^{2+} ions strongly, nothing could be generated if the reaction was halted immediately when the temperature reached 180 °C in the typical synthesis of Cu nanocubes. However, single-crystal seeds were formed after aging the mixed solution at 180 °C for 10 min (Fig. 3c). Cu nanocubes with truncated angles were obtained by prolonging the aging time to 30 min (Fig. 3d). A more prefect cubic morphology was formed once the aging time was increased to 2 h (Fig. S8†). From the EDS analysis, there is no Ni in the products at any stage. For comparison, trioctylphosphine oxide (TOPO) was used to replace TOP in the typical synthesis of Cu nanocubes. Both single-crystal and multi-twined seeds were formed during the initial stage, which can be ascribed to the fact that TOPO cannot coordinate with Ni^{2+} as strongly as TOP does. As a consequence, both Cu nanocubes and nanowires are present in the products (Fig. S9†). In summary, in the presence of TOP, the reduction rate of Ni^{2+} would become very slow owing to the formation of TOP–Ni^{2+} coordination complexes. Accordingly, the rate of the galvanic replacement between Ni^0 and Cu^{2+} was efficiently inhibited. Therefore, a slow nucleation and growth event from the reduced Cu monomers was guaranteed to ensure the complete generation of single-crystal seeds during the initial stage.[39] On the contrary, in the absence of TOP, Ni^{2+} ions were reduced into Ni^0 monomers rapidly without the ligand effect from TOP. Hence, Cu^{2+} ions were reduced rapidly by Ni^0 monomers during the galvanic replacement reaction. Under these conditions, which involved a burst of nucleation initiated by a high concentration of Cu monomers in the solution, multi-twinned seeds were formed rapidly during the initial stage, which then grew into five-fold twined pentagonal nanowires in the presence of a capping agent (Cl^-) though a ripening process. In an attempt to confirm that TOP does not have an observable effect on the shape of Cu NCs, controlled experiments using $Cu(NO_3)_2$ as a single precursor salt in the presence of different amounts of TOP were carried out for comparison (see ESI† for synthetic details). When the amount of TOP was changed from 0.5 to 3 ml, there was no observable difference in the morphology of the Cu NCs, and both of the products were spherical with a diameter of about 18 nm (Fig. S10†). In a word, TOP can be used to selectively generate different types of Cu crystal seeds through controlling the reduction rate of Ni^{2+}.

Surface adsorption of Cl^- ions

It should be noted that $CuCl_2$ not only serves as a Cu source but also provides abundant Cl^- ions after the reduction of the Cu^{2+} ions, which was shown to have a dramatic effect on the final shape of the NCs. In the following growth step, Cl^- ions serve as a capping agent that bond to the surface of the Cu crystal seeds, leading to the formation of nanocubes bound by six {100} facets or penta-twinned nanowires enclosed by mainly five {100} side facets. To confirm the coordination and chemisorption effect of Cl^- ions, $CuCl_2$ was substituted by $Cu(NO_3)_2$ as a single precursor salt (see ESI† for synthetic details), nanospheres instead of nanocubes or nanowires were generated (Fig. S11†). In an attempt to confirm the surface adsorption of the Cl^- ions, the Auger spectrum (Fig. 4) was monitored on the surface layer of the as-synthesized Cu nanocubes which had been washed five times with the mixed solution of hexane and methanol. Obviously, Cl and Cu can be detected on the surface of the products. The presence of the Cl peak in the Auger spectrum indicated that the surface of the Cu nanocubes was capped with Cl^- ions. A similar phenomenon was observed in the Auger spectrum of the Cu nanowires (Fig. S12†). On the other hand, the Auger

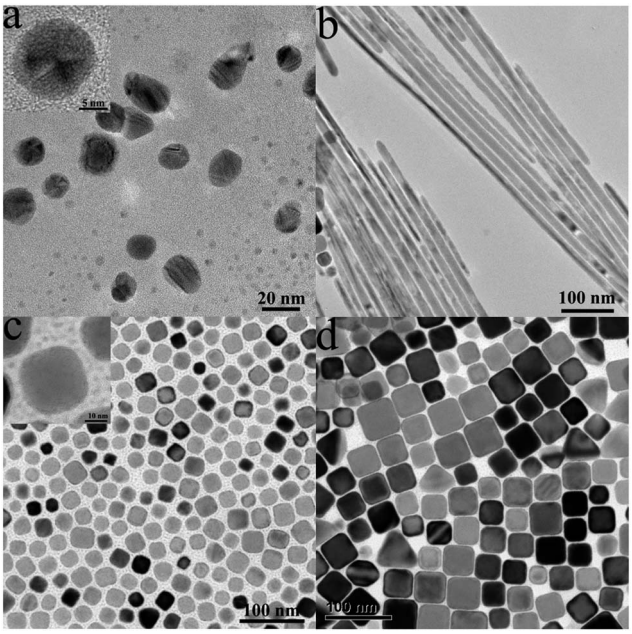

Fig. 3 TEM images of the samples formed at various time windows after the reaction temperature reaching 180 °C: (a) 0 min and (b) 10 min, other reaction conditions are the same as the typical route of Cu nanowire synthesis; (c) 10 min and (d) 30 min, other reaction conditions are the same as the typical route of the Cu nanocube synthesis. The insets in (a) and (c) are magnified images.

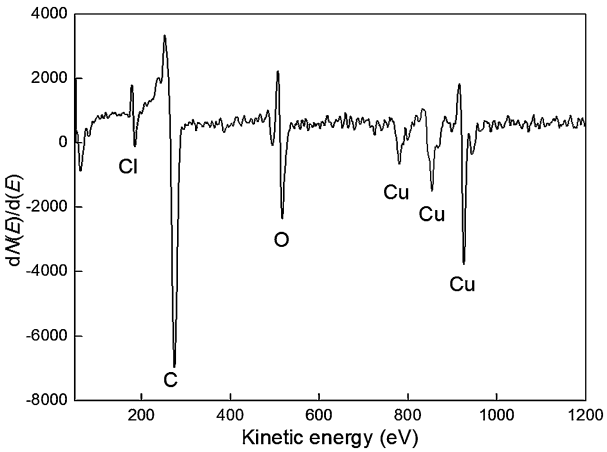

Fig. 4 Auger spectrum obtained from the surface of the as-synthesized Cu nanocubes in the derivative mode (d$N(E)$/dE).

spectrum in the range of 105–160 eV showed no peak assigned to P, which indicates that TOP does not adsorb on the surface of the Cu nanocubes or nanowires as strongly as the Cl^- ions do.

A similar result can be found in the IR spectrum of TOP and the as-prepared Cu nanocubes after washing once with the mixed solution of hexane and acetone (Fig. 5). In the FT-IR spectrum of TOP, the peaks at 1159, 1070 and 1023 cm^{-1}, which are assigned to the C–P stretching peaks of TOP,[40,41] can be observed obviously. However, these characteristic peaks of TOP disappear in the FT-IR spectrum of the as-prepared Cu nanocubes that have being washed only once. This confirms that TOP is relatively easy to wash off because of its weak adsorption. The two peaks located at 2920 and 2868 cm^{-1}, that correspond to the C–H stretching modes for the CH_2 and CH_3 groups, may originate from the alkane molecules adsorbed on the surface of the Cu NCs. The above results demonstrate that Cl^- ions have a much stronger adsorption ability than TOP on the surface of the Cu NCs, which may have essential influences in the evolvement of Cu NCs to a specific shape, though further work is needed to obtain more specific details.

Synthesis of Cu@Cu–Ni nanostructures

In the next step, we introduced ferromagnetic Ni as a coating metal to form a Cu–Ni alloy shell on the surface of the Cu NCs (named as Cu@Cu–Ni NCs in the following text), which made diamagnetic Cu NCs magnetically responsive. It should be noted that, no Ni could be detected from the EDS or Auger spectra in the as-prepared Cu NCs before the reaction temperature was increased to 210 °C, which indicated that pure Cu NCs were formed in the first step. However, owing to the presence of Ni^{2+} ions in the solution, coating the Cu NCs with a Cu–Ni alloy shell was very facile, which was achieved by increasing the reaction temperature to 210 °C. After the complete formation of the Cu NCs, a great deal of Cu^{2+} had been consumed.

Therefore, the concentration of Cu^{2+} would become very low. Under these conditions, highly active Ni^0 atoms reduced by oleylamine would partially deposit on the surface of the Cu NCs as well as reduce Cu^{2+} into Cu atoms which also deposited on the surface of the as-formed Cu NCs during galvanic replacement. As a result, a Cu–Ni alloy shell was formed on the surface of the Cu NCs to produce Cu@Cu–Ni nanostructures. Fig. 6a displays the TEM image of the as-synthesized Cu@Cu–Ni nanocubes which have an edge length of 81 ± 10 nm and contain 23 at% Ni (Fig. S13†). In order to confirm that the Ni–Cu alloy shell was formed during a heterogeneous nucleation process on the surface of the as-prepared Cu NCs, the composition of the time-dependent products in the shell formation process were analyzed by EDS. As shown in Table S1,† after the reaction temperature reached 220 °C, the atomic ratio of Ni would increase as the reaction proceeded. These results indicated that Cu NCs were formed in the first step, when the mixed solution was aged at 180 °C for 4 h, and then the Ni–Cu alloy shell would be formed at a higher temperature (220 °C). EDS line-scan analysis and mapping (Fig. 6b and c) performed in the scanning TEM (STEM) mode on an individual nanocube clearly indicate that Ni tends to exist at the cube edge while Cu is

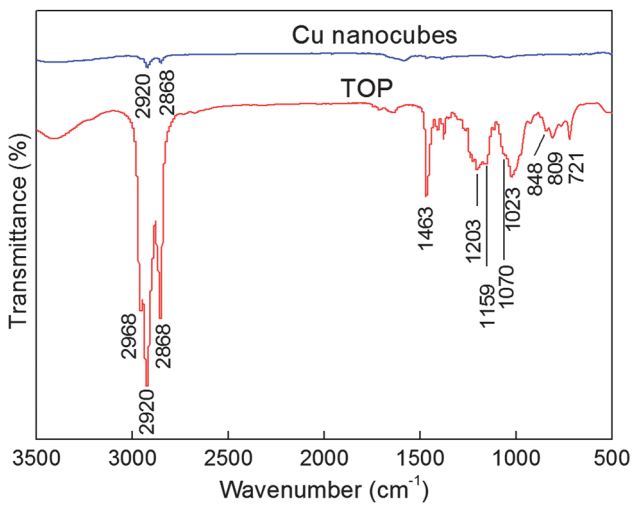

Fig. 5 FT-IR spectra of TOP and the as-prepared Cu nanocubes after washing once with the mixed solution of hexane and acetone.

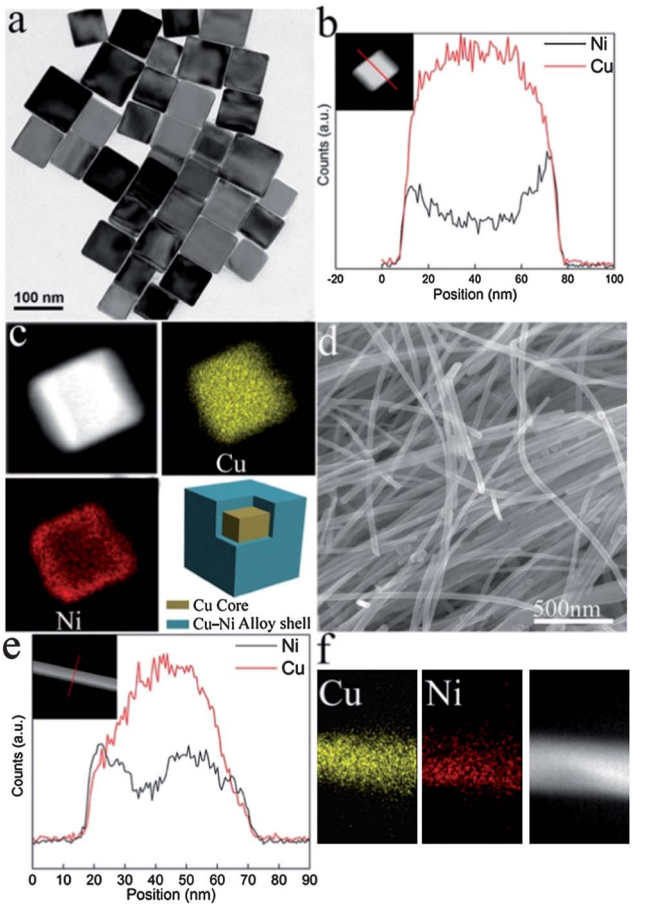

Fig. 6 (a) TEM image of the as-synthesized Cu@Cu–Ni nanocubes. (b) Elemental line profiles obtained from EDS line-scan analysis on a single nanocube (inset is the HAADF image). (c) HAADF image (top left), corresponding elemental maps (top right for Cu and bottom left for Ni) and graphic illustration (bottom right) of a Cu@Cu–Ni nanocube. (d) SEM image of the as-synthesized Cu@Cu–Ni nanowires. (e) and (f) are the elemental line profiles and maps of a single Cu@Cu–Ni nanowire, respectively.

concentrated more in the cube center. Both Ni and Cu are present at the edge, indicating a core–shell structure consisting of a Cu core and a Cu–Ni alloy shell. Fig. 6d displays the representative SEM image of the as-synthesized Cu@Cu–Ni nanowires which have an average diameter of 38 ± 3.6 nm and contain 28 at% Ni (Fig. S14†). EDS line-scan analysis and mapping (Fig. 6e and f) also reveal a core–shell structure with Cu in the wire centre and Cu–Ni at the wire edge. Since the Cu nanowires, which serve as a template to form a core–shell structure, have a smaller diameter size (22 nm) than its cubic counterpart, the homogenization process between Ni and Cu was improved, which led to thicker Cu–Ni alloy shells.

Optical properties

The Visible-NIR extinction spectra of the as-prepared Cu and Cu@Cu–Ni nanocubes and nanowires are displayed in Fig. 7; meanwhile, the spectra of the Cu nanospheres with a diameter of about 18 nm is included for comparison. According to the Mie scattering theory,[42] the absorption band of Cu NCs located in the UV-Vis range originates from the surface plasmon resonance (SPR), which is the coherent oscillation of the free conduction electrons induced by light. The Cu nanospheres exhibit a characteristic SPR band at 575 nm. However, the absorption band of the Cu nanocubes have a larger dimension of red-shifts to a longer wave length (625 nm). A similar phenomenon was observed in gold nanoparticles with different sizes.[43] On the other hand, the SPR band of the as-prepared Cu nanowires is located at 564 nm, as the transverse diameter of the Cu nanowires is smaller than that of the Cu nanospheres. As we have described before, the as-prepared Cu nanowires have a large length-to-diameter ratio with an average diameter of 15.2 nm and an entire length up to micrometer range. As a result, the position of the longitudinal plasmon resonance may red-shift to the spectrum region which is beyond the detection range of the UV-Visible-NIR spectrophotometer. Therefore, in the case of Cu nanowires, only the transverse SPR mode is observed. These results coincide well with the former observation of Jin *et al.*[29] The differences in the position of the SPR band of the Cu NCs is mainly due to the shape and size effect. It can also been noted that apart from the red-shift of the SPR band in the case of the Cu nanocubes there is an intensity increase too, which is related to the fact that the SPR band of the Cu nanocubes shifts away from the region of the interband transitions (below 590 nm). The Visible-NIR extinction spectra of the Cu@Cu–Ni nanocubes and nanowires are quite different from that of the pure Cu NCs. There is no obvious SPR band, which is due to the damping effects of Ni. Different from many noble metals, most transition metals have only a broad and poorly resolved absorption band in the ultraviolet region, which is attributed to the strong coupling between the plasmon transition and the d–d interband excitation. As a result, the plasmon energy is lost by excitation of the single electron interband transitions.[44] Such a damping effect of Ni has also been observed in our previous study on Ag@Ni and Au@Ni core–shell nanoparticles.[45,46]

Magnetic properties of Cu@Cu–Ni core–shell nanostructures

Magnetic measurements were carried out on the as-prepared Cu@Cu–Ni nanocubes and nanowires shown in Fig. 8 and the analytical results are summarized in Table S2.† The Cu@Cu–Ni nanocubes exhibit a magnetization of 0.8 emu g^{-1} at 50 kOe and do not show any hysteresis at 300 K; however, they show a ferromagnetic behavior with a coercivity of 12 Oe at 5 K and the magnetization at 50 kOe is 2.9 emu g^{-1} (Fig. 8a). The ZFC curve deviates from the FC curve at about 167 K (Fig. 8b) and shows a maximum at about 90 K, which indicates room-temperature superparamagnetic characteristics. The magnetizations of the as-synthesized Cu@Cu–Ni nanowires at 50 kOe are 3.0 and 0.4 emu g^{-1} at 5 and 300 K, respectively. The coercivity at 5 K is

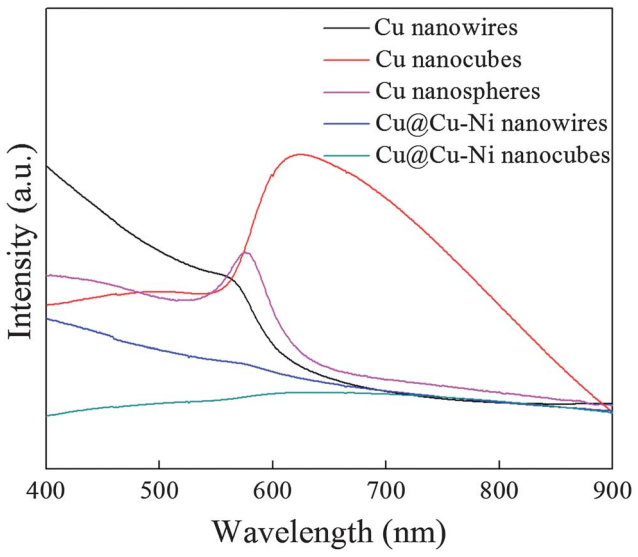

Fig. 7 Visible-NIR extinction spectra of the Cu nanospheres, nanocubes and nanowires, and Cu@Cu–Ni nanocubes and nanowires.

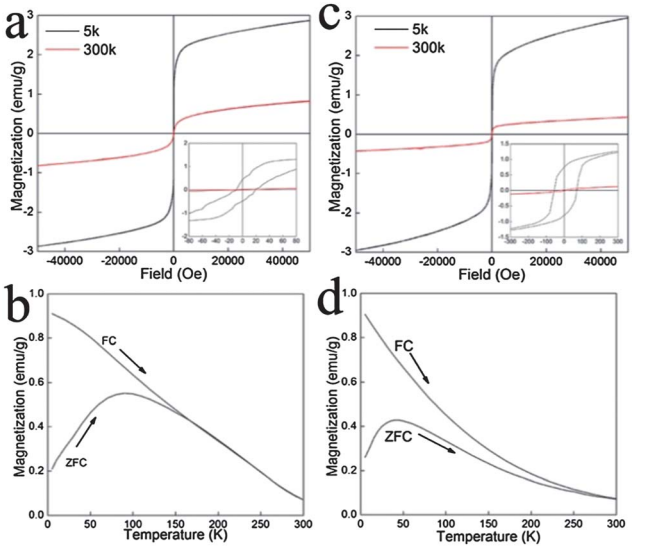

Fig. 8 Magnetic hysteresis loops (a) and ZFC–FC (100 Oe) curves (b) of the as-synthesized Cu@Cu–Ni nanocubes. Magnetic hysteresis loops (c) and ZFC–FC (100 Oe) curves (d) of the as-synthesized Cu@Cu–Ni nanowires.

70 Oe, but it decreases to 21 Oe at 300 K (Fig. 8c). Different from the Cu@Cu–Ni nanocubes, the FC and ZFC curves of the Cu@Cu–Ni nanowires do not coincide, even at temperatures reaching 300 K (Fig. 8d). This difference can be explained by the presence of a shape-anisotropic energy barrier that has to be overcome for the magnetic field to change the orientation of the magnetic moments. The symmetry of the nanowires is apparently lower than that of the nanocubes. Therefore, it is possible that the improved shape-anisotropic energy for the nanowires may contribute to the higher divergence temperature of the magnetization in the ZFC–FC measurements. A similar phenomenon was also observed for Ni nanosheets[10,14] and Ni–Cu nanoplates,[47] which had a higher divergence temperature in the ZFC–FC curves than their spherical counterparts. In addition, the shape-anisotropic effect may also contribute a larger coercivity to the Cu@Cu–Ni nanowires in comparison to their cubic counterparts. A significant enhancement in coercivity was also observed in Cu@Ni nanowires prepared *via* an aqueous method.[27] By growing Cu–Ni alloy shells over the Cu cores we have made the diamagnetic Cu NCs magnetically responsive and they can be directed to a desired location when an external magnetic field is applied (Fig. S15†). Furthermore, since Ni is more corrosion resistant than Cu, the incorporation of Ni on the surface of Cu NCs can enhance their anti-oxidation capacity, which is important for their practical applications.

Conclusions

In summary, we have developed a facile one-pot nonaqueous method for the shape-selective synthesis of Cu and Cu@Cu–Ni core–shell nanocubes and nanowires. The presence of Ni^{2+} and Cl^- ions, along with the assistance of TOP, play important roles in determining the final shape of the NCs. TOP can be used to selectively generate different crystal seeds that finally develop into nanocubes or nanowires, while Cl^- ions have been found to strongly adsorb on the surfaces of the Cu NCs, which may help maintain the morphologies of the NCs. The introduction of Cu–Ni alloy shells over the Cu cores greatly dampens the SPR band of the Cu NCs and makes the diamagnetic Cu NCs magnetically responsive. The as-prepared Cu@Cu–Ni nanocubes exhibit room-temperature superparamagnetic characteristics, whereas the Cu@Cu–Ni nanowires show a high divergence temperature in the ZFC–FC curves, which may be ascribed to the improved shape-anisotropic energy. The employed synthetic strategy may provide important clues for shape-controlled synthesis of other transition metal NCs, especially magnetic metal NCs. The as-prepared Cu and Cu@Cu–Ni NCs may hold widespread applications in the fields of microelectronics and magnetic recyclable catalysis.

Acknowledgements

The authors gratefully acknowledge financial support from the National Basic Research Program of China (no. 2012CB933103), the National Outstanding Youth Science Foundation of China (grant no. 50825101), and the National Natural Science Foundation of China (grant no. 51171157 and 50971108).

Notes and references

1 Y. Xia, Y. J. Xiong, B. Lim and S. E. Skrabalak, *Angew. Chem., Int. Ed.*, 2009, **48**, 60–103.
2 M. Chen, B. Wu, J. Yang and N. Zheng, *Adv. Mater.*, 2012, **24**, 862–879.
3 A. R. Tao, S. Habas and P. Yang, *Small*, 2008, **4**, 310–325.
4 R. Jin, Y. Cao, C. A. Mirkin, K. L. Kelly, G. C. Schatz and J. G. Zheng, *Science*, 2001, **294**, 1901–1903.
5 J. Zhang, M. R. Langille and C. A. Mirkin, *J. Am. Chem. Soc.*, 2010, **132**, 12502–12510.
6 F. Kim, S. Connor, H. Song, T. Kuykendall and P. Yang, *Angew. Chem., Int. Ed.*, 2004, **43**, 3673–3677.
7 K. M. Bratlie, H. Lee, K. Komvopoulos, P. Yang and G. A. Somorjai, *Nano Lett.*, 2007, **7**, 3097–3101.
8 X. Huang, S. Tang, X. Mu, Y. Dai, G. Chen, Z. Zhou, F. Ruan, Z. Yang and N. Zheng, *Nat. Nanotechnol.*, 2010, **6**, 28–32.
9 A. P. LaGrow, B. Ingham, S. Cheong, G. V. M. Williams, C. Dotzler, M. F. Toney, D. A. Jefferson, E. C. Corbos, P. T. Bishop, J. Cookson and R. D. Tilley, *J. Am. Chem. Soc.*, 2012, **134**, 855–858.
10 Y. Leng, Y. Li, X. Li and S. J. Takahashi, *J. Phys. Chem. C*, 2007, **111**, 6630–6633.
11 R. Xu, T. Xie, Y. Zhao and Y. Li, *Cryst. Growth Des.*, 2007, **7**, 1904–1911.
12 Y. Liu and A. R. H. Walker, *Angew. Chem., Int. Ed.*, 2010, **49**, 6781–6785.
13 Y. Xiong, J. M. McLellan, J. Chen, Y. Yin, Z.-Y. Li and Y. Xia, *J. Am. Chem. Soc.*, 2005, **127**, 17118–17127.
14 Y. Leng, Y. Wang, X. Li, T. Liu and S. Takahashhi, *Nanotechnology*, 2006, **17**, 4834.
15 B. Wiley, T. Herricks, Y. Sun and Y. Xia, *Nano Lett.*, 2004, **4**, 1733–1739.
16 G. Chen, Y. Tan, B. Wu, G. Fu and N. Zheng, *Chem. Commun.*, 2012, **48**, 2758–2760.
17 H. Zhang, M. Jin, J. Wang, W. Li, P. H. C. Camargo, M. J. Kim, D. Yang, Z. Xie and Y. Xia, *J. Am. Chem. Soc.*, 2011, **133**, 6078–6089.
18 S. Peng and Y. Sun, *Chem. Mater.*, 2010, **22**, 6272–6279.
19 G. Krylova, L. J. Giovanetti, F. G. Requejo, N. M. Dimitrijevic, A. Prakapenka and E. V. Shevchenko, *J. Am. Chem. Soc.*, 2012, **134**, 4384–4392.
20 P. Lignier, R. Bellabarba and R. P. Tooze, *Chem. Soc. Rev.*, 2012, **41**, 1708–1720.
21 A. R. Rathmell, S. M. Bergin, Y.-L. Hua, Z.-Y. Li and B. J. Wiley, *Adv. Mater.*, 2010, **22**, 3558–3563.
22 S. Schimpf, A. Rittermeier, X. Zhang, Z.-A. Li, M. Spasova, M. W. E. van den Berg, M. Farle, Y. Wang, R. A. Fischer and M. Muhler, *ChemCatChem*, 2010, **2**, 214–222.
23 J. B. Park, J. Graciani, J. Evans, D. Stacchiola, S. D. Senanayake, L. Barrio, P. Liu, J. F. Sanz, J. Hrbek and J. A. Rodriguez, *J. Am. Chem. Soc.*, 2009, **132**, 356–363.
24 Y. Zhang, W. Huang, S. E. Habas, J. N. Kuhn, M. E. Grass, Y. Yamada, P. Yang and G. A. Somorjai, *J. Phys. Chem. C*, 2008, **112**, 12092–12095.
25 W. Chen, R. Yu, L. Li, A. Wang, Q. Peng and Y. Li, *Angew. Chem., Int. Ed.*, 2010, **49**, 2917–2921.

26 T. Yamauchi, Y. Tsukahara, T. Sakata, H. Mori, T. Yanagida, T. Kawai and Y. Wada, *Nanoscale*, 2010, **2**, 515–523.
27 S. Zhang and H. C. Zeng, *Chem. Mater.*, 2010, **22**, 1282–1284.
28 M. Tsuji, D. Yamaguchi, M. Matsunaga and M. J. Alam, *Cryst. Growth Des.*, 2010, **10**, 5129–5135.
29 M. Jin, G. He, H. Zhang, J. Zeng, Z. Xie and Y. Xia, *Angew. Chem., Int. Ed.*, 2011, **50**, 10560–10564.
30 L. Lu, Y. Shen, X. Chen, L. Qian and K. Lu, *Science*, 2004, **304**, 422–426.
31 E. Ye, S.-Y. Zhang, S. Liu and M.-Y. Han, *Chem.–Eur. J.*, 2011, **17**, 3074–3077.
32 X. Huang and N. Zheng, *J. Am. Chem. Soc.*, 2009, **131**, 4602–4603.
33 Y. Sun and Y. Xia, *Adv. Mater.*, 2002, **14**, 833–837.
34 Y. Chen, D. L. Peng, D. X. Lin and X. H. Luo, *Nanotechnology*, 2007, **18**, 505703.
35 Y. Sun, B. T. Mayers and Y. Xia, *Nano Lett.*, 2002, **2**, 481–485.
36 Y. Sun, B. Mayers and Y. Xia, *Adv. Mater.*, 2003, **15**, 641–646.
37 W. Zhang, J. Yang and X. Lu, *ACS Nano*, 2012, **6**, 7397–7405.
38 K. W. Kim, S. M. Kim, S. Choi, J. Kim and I. S. Lee, *ACS Nano*, 2012, **6**, 5122–5129.
39 Y. Tang and M. Ouyang, *Nat. Mater.*, 2007, **6**, 754–759.
40 S. Chen, X. Zhang, Q. Zhang and W. Tan, *Nanoscale Res. Lett.*, 2009, **4**, 1159–1165.
41 X. Lu, B. A. Korgel and K. P. Johnston, *Chem. Mater.*, 2005, **17**, 6479–6485.
42 G. Mie, *Ann. Phys.*, 1908, **25**, 377–445.
43 S. Link and M. A. EI-Sayed, *J. Phys. Chem. B*, 1999, **103**, 4212–4217.
44 P. Mulvaney, *Langmuir*, 1996, **12**, 788–800.
45 H. Guo, Y. Chen, X. Chen, R. Wen, G.-H. Yue and D.-L. Peng, *Nanotechnology*, 2011, **22**, 195604.
46 H. She, Y. Chen, X. Chen, K. Zhang, Z. Wang and D.-L. Peng, *J. Mater. Chem.*, 2012, **22**, 2757–2765.
47 H. Guo, Y. Chen, H. Ping, L. Wang and D.-L. Peng, *J. Mater. Chem.*, 2012, **22**, 8336–8344.

